ELSEVIER

Contents lists available at ScienceDirect

European Journal of Control

journal homepage: www.sciencedirect.com/journal/european-journal-of-control



Artificial neural network based iterative learning control for stroke rehabilitation

Xiaoru Sun[®], Chris T. Freeman[®]*

School of Electronics and Computer Science, University of Southampton, University Road, Southampton, SO17 1BJ, Hampshire, UK

ARTICLE INFO

Recommended by T. Parisini

Keywords: Iterative learning control Artificial neural network Functional electrical stimulation Stroke rehabilitation

ABSTRACT

An artificial neural network (ANN) is combined with gradient descent to form a model-free iterative learning control (ILC) approach than can be applied to a wide range of nonlinear discrete-time systems. The ANN is recursively trained on the entire set of past data collected from the system and uses a passivity condition to determine when the ANN can be used to compute the next ILC update, or if an identification test is needed. Convergence properties are established alongside design selections that ensure the passivity condition is fulfilled. By minimising the reliance on identification tests, this methodology is substantially faster than existing model-free ILC algorithms. It is tested on a key stroke rehabilitation problem using functional electrical stimulation (FES) for hand/wrist tracking. Experimental results using the new ILC approach with eight participants show that three hand/wrist references can be tracked using an average of 56% fewer experimental inputs compared with the most accurate previous approach. As the first approach to combine ILC and machine learning in upper limb rehabilitation, the results demonstrate how their combination addresses their individual deficiencies.

1. Introduction

Stroke is a leading cause of death and disability worldwide (Feigin et al., 2022) and is the result of a loss of blood flow in regions of the brain. Approximately 70% of stroke survivors experience upper limb dysfunction, and only a small fraction fully recover (Eraifej, Clark, France, Desando, & Moore, 2017). In 2022, the global cost of stroke was \$891 billion, and the economic impact will continue rising without strong prevention, healthcare, and rehabilitation strategies (Saposnik et al., 2022).

Rehabilitation consists of the patient repeatedly performing a functional task, such as reaching to push a switch or grasp an object. The sensory feedback they receive (proprioceptive, haptic, and visual) then helps them to re-learn lost movement via neuroplasticity. Early, intensive functionally-oriented therapy can deliver a long-lasting improvement to motor function (Ballester et al., 2022), and the 2023 stroke clinical guidelines recommend patients receive at least 3 hours per day (Intercollegiate Stroke Working Party; London, 2023). However current provision consists of mainly manual assistance from a therapist for only half an hour, three times per week (Stockley, Peel, Jarvis, & Connell, 2019). Therefore, rehabilitation technologies are urgently needed to deliver the high doses of therapy required.

Functional electrical stimulation (FES) is the most widely used rehabilitation technology, and involves placing electrode pads on the skin

through which electrical impulses are applied to artificially stimulate the underlying muscles (Hughes et al., 2014). If adequately controlled, FES enables patients to practice movements and relearn their lost sensorimotor function. FES has substantial clinical evidence (Eraifej et al., 2017) and is strongly recommended by the UK National Clinical Stroke Guidelines (Crow & Smith, 2023).

Commercial FES systems use large electrode pads, with stimulation delivered using pre-set openloop profiles. This means they cannot precisely activate the numerous upper limb and forearm muscles essential for dexterous arm and hand motion (Marquez-Chin, Kapadia-Desai, & Kalsi-Ryan, 2021). To overcome this problem, FES electrode arrays have recently emerged and comprise multiple electrode pads arranged in a single structure. Recent examples are low cost, washable, and can even be integrated in everyday clothing (Yang et al., 2018). However, their control is still challenging due to the large number of muscles in the forearm, their sensitivity to array positioning, the complexity of the tendon network and coupled musculoskeletal dynamics, and day-to-day variation in physiological response to stimulation.

The majority of controllers for FES arrays manually select electrode pads based on visual assessment of the resulting movements (Bijelić, Popović-Bijelić, Jorgovanović, Bojanić, & Popović, 2004), or measurement of joint angle deviation (O'Dwyer, O'Keeffe, Coote, & Lyons,

E-mail addresses: xs1a12@soton.ac.uk (X. Sun), cf@ecs.soton.ac.uk (C.T. Freeman).

^{*} Corresponding author.

2006). This process has been automated by stimulating each array pad in turn to find the one producing most force (Popović & Popović, 2009; Schill, Rupp, Pylatiuk, Schulz, & Reischl, 2009), taking 10 min. Later modifications used combinations of electrodes (Hoffmann, Deinhofer, & Keller, 2012), the muscle twitch response (Malešević et al., 2012), points specified by therapists (Popović-Maneski et al., 2013), and electromyography (De Marchis, Santos Monteiro, Simon-Martinez, Conforto, & Gharabaghi, 2016; Maneski et al., 2016) to reduce the search time. However, the resulting movement was still crude, and took several minutes.

1.1. FES array control approaches

Few model-based feedback approaches have been used due to the difficulty in modelling and identifying the complex, high dimensional system dynamics. The exception is ILC, which has a long history of use in FES based rehabilitation (Freeman, 2016). ILC uses data from previous attempts of a repeated tracking task to update the control signal applied in the current attempt. This matches the rehabilitation process exactly, and this connection has led to ILC being used in multiple clinical studies with stroke patients (Freeman, 2016).

When applied to FES arrays, ILC has delivered higher accuracy than all other approaches (Freeman, 2014; Yang et al., 2018), (mean joint error < 5° for pointing, pinch and open hand movements). However, the absence of a reliable model meant it required identification tests to be performed between each ILC update. It therefore took 10 min to track each hand gesture, and it must be repeated when the FES array is moved. This is still too long for clinical or home use. To reduce this time, Sun and Freeman (2024b) developed an ILC algorithm that used a piecewise mapping model which was recursively updated to replace the identification procedure. However it required that experimental data points had been collected in every segment of the mapping domain, meaning that a large amount of data was needed for multiple stimulation channels.

Aside from ILC, few advanced control approaches have been applied to FES arrays. An exception is (Imatz-Ojanguren, Irigoyen, Valencia-Blanco, & Keller, 2016), in which a recurrent fuzzy artificial neural network (ANN) was trained to map between a 16 element FES array and the resulting wrist/finger angles. Experimental results showed accuracy of over 60%. However, the training data (comprising randomised pulses) were uncomfortable to patients and could only capture simple movements. Data were also collected by an instrumented glove which cannot be worn by most patients. The training took 45 min and would need repeating for each treatment session.

1.2. Artificial neural network-based ILC

An obvious route is to harness the ability of machine learning to learn complex dynamics, while retaining the ability of ILC to use minimum data, retain precise control of inputs, embed implicit interpretability, and benefit from rigorous theoretical convergence properties.

Integrating ILC and ANNs has not been applied to FES arrays, but has been proposed by several authors. In Wang and Chien (2012) an adaptive neural ILC update employed an output recurrent NN to estimate plant nonlinearities via online learning, but required full state measurements and stability conditions that are difficult to guarantee in practical applications. A similar approach in Chen and Wen (2020) proposed a neural-network-enhanced ILC method that approximated inverse system dynamics via offline learning. Similarly, Liu, Wang, and Chi (2015) used a radial basis function neural network to represent nonlinear plant dynamics in an adaptive ILC scheme. However, all these methods required high-dimensional, dense datasets, are not designed for multiple task generalisation, and lack theoretical guarantees on convergence or robustness.

A closely related field is that of optimization-based data-driven ILC. While many such approaches assume linear dynamics (He et al., 2022; Soleimani, Sedigh, & Nikoofard, 2025; Tian et al., 2025; Zhang & Zou, 2024), others have been developed for nonlinear systems. Several of these employ extra experiments to generate the update signals used by each ILC update (Huo, Freeman, & Liu, 2020; Lee, Cheng, Yuan, & Tsao, 2025; Lee, Rai, & Tsao, 2022), however the additional experiments quickly become prohibitively time-consuming for MIMO systems. Other data-driven schemes adaptively update a parameterised model of the nonlinear system (Chi, Hou, Huang, & Jin, 2015; Chi, Hou, Jin, & Huang, 2018; Chi, Li, Lin, & Huang, 2024; Zhu & Hou, 2014), which is often combined with dynamic linearisation to simplify the control action that is subsequently applied. While successful in many cases, limitations have been pointed out by several authors (He et al., 2022; Hu et al., 2024; Huang & Huang, 2024; Xu, Meng, & Wang, 2024): the dynamics are typically required to be SISO; performance is often sensitive to initial parameter selection; to avoid slow convergence historical data is needed to pre-train the model; tuning parameters/weights can be challenging; and learning multiple references has not been considered. A further limitation is a lack of transparency: e.g. there is no simply test to decide whether more training data are needed to smooth transients (which may be problematic in applications involving human subjects).

1.3. Contributions

The current paper introduces a neural ILC framework that combines the capability of ANNs to learn complex dynamics with the rigorous performance guarantees of model-free ILC. It is the first combination of ILC and machine learning for FES control, and addresses the limitations of prior attempts to combine these methods. It builds on the ILC approach of Sun and Freeman (2024b), but significantly reduces the amount of data required by exchanging piecewise linear mappings for ANN structures. These provide greater efficiency, while guaranteeing convergence to minimal error. Furthermore, we provide transparent convergence conditions that inform ANN design and learning gain selection, extending previous machine-learning-based FES control approaches with theoretical assurances. Initial results appeared in Sun and Freeman (2024a) but did not include full proofs, hardware development, implementation, or practical validation results. To summarise, the contributions of this paper are:

- It develops the first framework combining ILC and ANNs to be applied to FES based rehabilitation, with results confirming a significant reduction in the amount of data required to achieve hand and wrist gestures compared with all previous controllers.
- It is the first combined ILC and ANN framework to support tracking of multiple reference trajectories. It also introduces theoretical performance guarantees to significantly reduce the amount of data required for ANN training compared to existing methods combining ILC and ANNs.
- Experimental results with eight participants demonstrate that its matches the best existing hand and wrist tracking performance, while using 56% fewer experimental tests than previous ILC schemes.
- Experiments employ low-cost control and sensing suitable for home deployment with patients. This is the only example of using 3D depth cameras for FES tracking control, and demonstrates feasibility.

The next section introduces the problem description.

2. Problem description

A general form of m-input, p-output nonlinear discrete-time system is considered, and is defined by

$$x(t+1) = f(x(t), u(t)), \quad x(0) = x_0,$$

$$v(t) = h(x(t)), t = 0, 1, ..., N - 1$$
 (1)

where, $x(t) \in \mathbb{R}^q$ is the state, $u(t) \in \mathbb{R}^m$ is the input, $y(t) \in \mathbb{R}^p$ is the output and t is the sample index.

Assumption 1. The vector functions $f(\cdot)$ and $h(\cdot)$ are continuously differentiable with respect to their arguments.

This assumption and the general form (1) is common in ILC literature (Huo et al., 2020; Lin, Owens, & Hätönen, 2006), and also encompasses a wide range of biomechanical systems used to design rehabilitation and assistive technologies (Freeman, 2016; Freeman et al., 2009). The fundamental tenet of ILC is that the system repeatedly performs a tracking task over a fixed time duration of N samples. Each attempt is termed a trial and is denoted by adding a subscript $k \in \mathbb{N}_+$ to each signal in (1). A second fundamental assumption is:

Assumption 2. The system resets to identical initial conditions between each trial, i.e. $x_k(0) = x_0$.

This is used in the vast majority of ILC research and is usually trivial to satisfy for industrial processes. However, it may be more difficult in other domains, especially those involving humans. The effect of non-identical initialisation has therefore been studied in many papers, including (Owens, Freeman, & Chu, 2014).

Given its fixed trial duration, it is standard practice in ILC to compactly represent the system using the super-vectors

$$\boldsymbol{u} = \begin{bmatrix} u(0)^{\mathsf{T}}, & u(1)^{\mathsf{T}}, & \dots & u(N-1)^{\mathsf{T}} \end{bmatrix}^{\mathsf{T}} \in \mathbb{R}^{mN},$$
 (2)

$$\mathbf{y} = \begin{bmatrix} y(1)^{\mathsf{T}}, & y(2)^{\mathsf{T}}, & \dots & y(N)^{\mathsf{T}} \end{bmatrix}^{\mathsf{T}} \in \mathbb{R}^{pN}, \tag{3}$$

$$\mathbf{r} = \begin{bmatrix} r(1)^{\mathsf{T}}, & r(2)^{\mathsf{T}}, & \dots & r(N)^{\mathsf{T}} \end{bmatrix}^{\mathsf{T}} \in \mathbb{R}^{pN}.$$
 (4)

This enables dynamics (1) to be expressed as the vector mapping $\mathbf{y} = \mathbf{g}(\mathbf{u}) : \mathbb{R}^{mN} \to \mathbb{R}^{pN}$ where $\mathbf{g}(\mathbf{u}) = [g_1(\mathbf{u})^\top, \dots g_N(\mathbf{u})^\top]^\top$ has the $t = 1, \dots N$ elements

$$\begin{split} g_t(x(0), u(0), \dots u(t-1)) &= h(x(t)) \\ &= h(f(x(t-1), u(t-1))), \\ &= h(f(f(x(t-2), u(t-2)), u(t-1))), \\ &\vdots \\ &= h(f(f(\dots f(x(0), u(0)), \dots, u(t-2)), u(t-1))). \end{split}$$

Although in conventional ILC the system output y_k tracks a single reference trajectory, for successful rehabilitation the patient must practice a range of tasks in a single treatment session. They attempt each task multiple times, with a therapist moving their arm back to a starting position (Freeman, 2016). Once they have completed each task adequately well (as determined by the therapist), they then move on to the next.

The control objective is therefore to track each reference using the minimum number of ILC attempts. Since perfect tracking is infeasible in practice, a prescribed upper limit on the tracking error will be used. Enforcing a minimum number of ILC trials means that the optimum assistance is found rapidly which maximises the patient benefit. In practice, the number of attempts of each task will be decided by the therapist and is typically between eight and ten.

No information about the system is available since the stimulated arm dynamics are highly dependent on set-up and physiological conditions that vary widely between sessions, and identification tests are not possible. However all data collected while attempting to track previous tasks can be used to track the next reference trajectory.

This gives rise to the following control objective:

Definition 1 (*ILC Multi-Reference Tracking Objective*). Define a set of n reference trajectories, $\mathcal{R} = \{r_1, r_2, \dots, r_n\}$. For each $r_i \in \mathcal{R}$ in turn, the ILC algorithm must compute a sequence of control inputs, $\{u_k\}_{k=0,1,\dots}$

that will converge to the solution u_i^* which minimises the tracking error, i.e.

$$\lim_{k \to \infty} u_k = u_i^*, \quad u_i^* := \arg\min_{u} J_i(u),$$

$$J_i(u) = \left\| \mathbf{r}_i - \mathbf{g}(u) \right\|^2$$
(5)

The ILC algorithm has no knowledge of system dynamics (1), but has access to all input–output data measured when tracking the preceding references $r_1, \dots r_{i-1}$.

The minimum number of trials required to track r_i with an accuracy of δ is defined by

$$k_{i,\delta} := \min\{k : \left| J_i(\boldsymbol{u}_k) - J_i(\boldsymbol{u}^*) \right| < \delta\}. \tag{6}$$

and the aim is to minimise the total number of trials needed to track all references with an accuracy of δ , i.e.

$$\min k_{\delta}, \quad k_{\delta} := \sum_{i=1}^{n} k_{i,\delta}. \tag{7}$$

3. ILC application

The performance of the most common ILC approach used in FES-based rehabilitation, see for example (Freeman, 2014; Lin et al., 2006; Yang et al., 2018), is now analysed. This class of ILC has been successfully applied in several upper limb clinical studies with stroke patients (Freeman, 2016). The algorithm is intended to track one reference, r_i , using the update form

$$u_{k+1} = u_k + L(r_i - y_k)$$
 (8)

where $\mathbf{y}_k = \mathbf{g}(\mathbf{u}_k)$ is generated by performing an experiment, and $L \in \mathbb{R}^{pN \times mN}$ is a learning operator that is designed based on the system dynamics \mathbf{g} . When it was applied to FES electrode arrays (Freeman, 2014), the choice

$$L = \gamma (\mathbf{g}'(\mathbf{u}_k))^{\mathsf{T}},\tag{9}$$

was made, where γ is a positive scalar. Update (9) has a simple interpretation: it is the gradient based iterative minimisation of $J_i(u) = \|\mathbf{r}_i - \mathbf{g}(u)\|^2$, which has desirable properties including convergence to minimal error and monotonic error norm reduction. Although there are many alternatives including inverse (Lin et al., 2006) and norm-optimal ILC, gradient ILC's superior robustness margins have made it the most popular model-based approach used in rehabilitation (Freeman, 2016). Computing L requires knowledge of the local system model computed about each new ILC signal, given by

$$g'(u_k) := \frac{\delta g(u)}{\delta u} \bigg|_{u=u_k} = \begin{bmatrix} \frac{\delta g_1(u)}{\delta u_1} \bigg|_{u=u_k} & \dots & \frac{\delta g_1(u)}{\delta u_m} \bigg|_{u=u_k} \\ \vdots & \ddots & \vdots \\ \frac{\delta g_p(u)}{\delta u_1} \bigg|_{u=u_k} & \dots & \frac{\delta g_p(u)}{\delta u_m} \bigg|_{u=u_k} \end{bmatrix}$$
(10)

 $\in \mathbb{R}^{mN \times pN}$. In Freeman (2014) and Yang et al. (2018) it was assumed $g(u_k)$ was unknown and must be identified experimentally. The authors proposed finding $g'(u_k)$ by solving the identification problem

$$g'(u_k) = \arg\min_{X} J(X), \quad J(X) = \|\Delta y - X\Delta u\|^2$$
(11)

where $X \in \mathbb{R}^{pN \times mN}$ with $(\Delta u, \Delta y)$ chosen to sufficiently excite the system dynamics about (u_k, y_k) . Here $\Delta u = u - u_k$, $\Delta y = y - g(u_k)$ are the deviation from the operating point and (u, y) are the experimental input and output signals. Algorithm 1 summarises the overall procedure. Here an inner loop has been added to track each reference from set \mathcal{R} , with the inner learning process starting from the same initial input u_0 for each $r_i \in \mathcal{R}$. Algorithm 1 corresponds to the approach that was applied to FES arrays in Freeman (2014), Ward et al. (2020) and Yang et al. (2018). In these studies, three references were tracked, and an initial input of $u_0 = \mathbf{0}$ was used for each one.

Algorithm 1 Standard ILC for multiple references

```
Require: Reference r_i \in \mathcal{R}, accuracy margin \delta for i=1:n do  \text{Set } k=0. \text{ Select starting input, } u_0, \text{ for reference } r_i. \\  \text{while } \left|J_i(u_k)-J_i(u^*)\right|<\delta \text{ do} \\  \text{Apply } u_k \text{ experimentally, record } y_k=g(u_k). \\  \text{Identify } g'(u_k) \text{ experimentally by applying input } u \text{ and solving } \\  (11). \\  \text{Compute new ILC update using (8).} \\  k=k+1 \\  \text{end while} \\  \text{end for}
```

3.1. Convergence results

The need for repeated identification tests means that standard ILC requires many experiments to be performed. To quantify this, the relationship between the number of tests and the resulting accuracy (i.e. parameters k, δ in (6)) is now derived. ILC update (9) will be focused upon, due to its mathematical tractability. However, no ILC convergence conditions exist for (9), so they are now derived. The next result also bounds the number of ILC trials required to track the entire set of n references, \mathcal{R} .

Theorem 1. Suppose function g(u) is differentiable and for each $r_i \in \mathcal{R}$ the error norm $J_i(u) := \|r_i - g(u)\|^2$ has a Lipschitz continuous gradient with constant L > 0. Suppose ILC update (9) is applied to track all references in \mathcal{R} each time starting from the same initial input u_0 . Then Algorithm 1 using ILC update (9) yields an error norm sequence $\{\|r_i - y_k\|^2\}_{k=0,1,\ldots}$ that converges to a local minimum provided the learning gain is chosen to satisfy

$$0 < \gamma < 4/L. \tag{12}$$

If $J_i(u)$ is also convex, this is a global minimum. An upper bound on the number of trials needed to satisfy (6), (7) is

$$k_{\delta} \le \sum_{i=1}^{n} \frac{\|u_0 - u_i^*\|^2}{2\gamma \delta}.$$
 (13)

Proof. Follows from Theorem 1 and 2 in Sun and Freeman (2024b).

Theorem 1 confirms that (9) can be used to solve the ILC multi-reference tracking objective of Definition 1, under mild assumptions matching (Lin et al., 2006). However it also confirms the prohibitively large number of trials required by current ILC approaches, since Algorithm 1 may take $\sum_{i=1}^n \frac{\|u_0-u_i^*\|^2}{2\gamma\delta}$ trials to track all references and δ is likely to be small. Clearly choosing u_0 close to the optimal value u_i^* for each reference directly reduces the number of trials required, however there is no way of achieving this in the absence of model information. This is addressed in the next section.

4. Artificial neural network based ILC

In Algorithm 1, the identification of $g'(u_k)$ must be repeated for each new trial and reference trajectory. This process is too time-consuming for applications such as stroke rehabilitation. While Algorithm 1 generates substantial data as it is applied to n references, a natural idea is to use these data to reduce the number of identification tests needed. This will done by fitting an ANN to the collected input—output data, and using it to replace the identification of $g'(u_k)$ within each update. The ANN will also be used to compute an optimal starting input for each new reference. In this way, applying ILC to the current reference helps speed up the learning of future references since the data generated increases the accuracy of the ANN model.

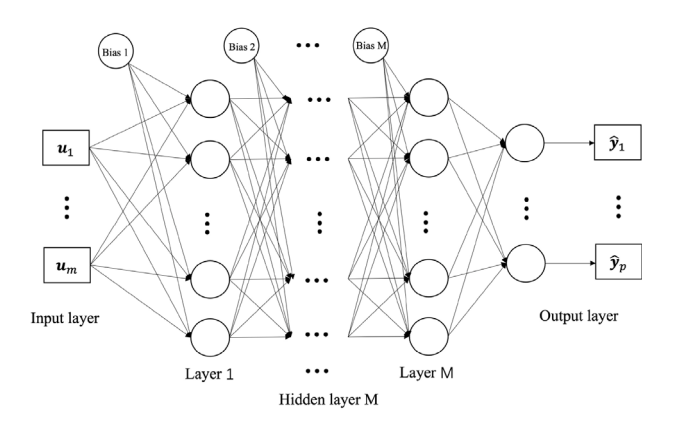


Fig. 1. Feed forward ANN structure with M hidden layers.

Consider a feed-forward ANN structure with M hidden layers, where the ith layer has M_i neurons, followed by an output function, as shown in Fig. 1. This can be expressed by the general vector mapping form

$$\hat{\mathbf{y}} = \bar{\mathbf{g}}(\mathbf{u}, \boldsymbol{\theta}) : (\mathbb{R}^{mN} \times \mathbb{R}^{\nu}) \to \mathbb{R}^{pN}, \tag{14}$$

where parameter vector $\theta \in \mathbb{R}^v$ contains the ANN weights and biases. This simple form is chosen as it leads to a transparent convergent condition that is underpinned by theory.

Suppose a set of existing input—output data have been stored from running previous experiments and are denoted $\{u_i, y_i\}_{i=1,2,...}$. These may have been generated by applying ILC to track previous references and it may also include data produced by applying ILC to track the current reference. Then back propagation training methods can be applied to compute the optimal vector θ by minimising a suitable function of the fitting error, e.g.

$$\hat{\theta} := \min_{\theta} \sum_{i} \|\mathbf{y}_{i} - \bar{\mathbf{g}}(\mathbf{u}_{i}, \theta)\|^{2}. \tag{15}$$

When new experimental data become available, the ANN model parameters can be updated using efficient recursive forms. If the form $\bar{g}(u,\theta)$ is sufficiently accurate, it can be used in (8)–(10) to replace the identification step in Algorithm 1. The next result quantifies the necessary accuracy.

Theorem 2. Suppose an ANN structure $\bar{g}(u, \theta)$ is chosen to approximate the system dynamics g(u). Let g(u), $J_i(u)$ satisfy the conditions of Theorem 1. If

$$\mathbf{g}'(\mathbf{u})^{\mathsf{T}}\bar{\mathbf{g}}'(\mathbf{u},\theta) > 0 \tag{16}$$

then the ANN based ILC gradient update

$$\mathbf{u}_{k+1} = \mathbf{u}_k + \gamma_k (\bar{\mathbf{g}}'(\mathbf{u}_k, \boldsymbol{\theta}))^{\mathsf{T}} (\mathbf{r}_i - \mathbf{y}_k)$$
(17)

applied to the system g(u) converges to the minimum error norm provided the ILC gain is chosen to satisfy

$$0 < \gamma_k < \frac{2e_k^\top g'(u_k)(\bar{g}'(u_k, \theta))^\top e_k}{L\|\bar{J}_i'(u_k, \theta)\|^2}$$
 (18)

where L is the Lipschitz constant and $e_k = r - g(u_k)$. If $J_i(u)$ is convex, this is the global minimum error norm.

Proof. Lipschitz continuity guarantees that

$$J_i(u_{k+1}) \le J_i(u_k) + J_i'(u_k)^{\mathsf{T}}(u_{k+1} - u_k) + ||u_{k+1} - u_k||^2 \frac{L}{2}$$

and substituting $\bar{J}_i'(u_k,\theta) := -2\bar{g}'(u_k,\theta)^{\top}(r_i - g(u_k))$ in the ANN based ILC update yields

$$\boldsymbol{u}_{k+1} = \boldsymbol{u}_k + 2\gamma(\bar{\boldsymbol{g}}'(\boldsymbol{u}_k, \boldsymbol{\theta}))^{\mathsf{T}}(\boldsymbol{r}_i - \boldsymbol{g}(\boldsymbol{u}_k)). \tag{19}$$

It then follows that

$$\begin{split} J_{i}(u_{k+1}) &\leq J_{i}(u_{k}) + J_{i}'(u_{k})^{\top}(u_{k} - \gamma \bar{J}_{i}'(u_{k}, \theta) - u_{k}) \\ &+ \|u_{k} - \gamma \bar{J}_{i}'(u_{k}, \theta) - u_{k}\|^{2} L/2 \\ &= J_{i}(u_{k}) - \gamma J_{i}'(u_{k})^{\top} \bar{J}_{i}'(u_{k}, \theta) + \gamma^{2} \|\bar{J}_{i}'(u_{k}, \theta)\|^{2} L/2. \end{split}$$

The term $J'_i(u_k)^{\top} \bar{J}'_i(u_k, \theta)$

$$=4(\mathbf{r}_i-\mathbf{g}(\mathbf{u}_k))^{\mathsf{T}}\mathbf{g}'(\mathbf{u}_k)(\bar{\mathbf{g}}'(\mathbf{u}_k,\boldsymbol{\theta}))^{\mathsf{T}}(\mathbf{r}_i-\mathbf{g}(\mathbf{u}_k))$$
(20)

is strictly positive if assumption (29) holds, i.e.

$$\mathbf{g}'(\mathbf{u}_k)\bar{\mathbf{g}}'(\mathbf{u}_k,\theta)^{\mathsf{T}} > 0, \qquad \forall \mathbf{u}_k \neq \mathbf{u}^*.$$
 (21)

Next denote $a_k := J'_i(\mathbf{u}_k)^{\top} \bar{J}'_i(\mathbf{u}_k, \theta)$ and select

$$0 < \gamma < \frac{2a_k}{L\|\bar{J}_i'(\boldsymbol{u}_k, \boldsymbol{\theta})\|^2} \tag{22}$$

so that the previous inequality becomes $J_i(\mathbf{u}_{k+1})$

$$\begin{split} J_i(\boldsymbol{u}_{k+1}) &\leq J_i(\boldsymbol{u}_k) - \gamma \bigg(J_i'(\boldsymbol{u}_k)^\top \bar{J}_i'(\boldsymbol{u}_k, \boldsymbol{\theta}) \\ &- \gamma \|\bar{J}_i'(\boldsymbol{u}_k, \boldsymbol{\theta})\|^2 \frac{L}{2} \bigg) \\ &< J_i(\boldsymbol{u}_k). \end{split} \tag{23}$$

It is always possible to select $\gamma = \frac{a_k}{L \|\bar{J}_i'(u_k, \theta)\|^2}$, then

$$J_i(u_{k+1}) < J_i(u_k) - \gamma \frac{a_k}{2}. \tag{24}$$

Since $a_k>0 \ \forall \ r_i-g(u_k)\neq 0$, (24) implies a reduction in tracking error norm with each trial of gradient ILC until the optimal value is attained, i.e. $J_i(u_k)=J_i(u^*)=0$. \square

Theorem 2 provides a simple condition on the ANN form $\bar{g}(u_k,\theta)$ which allows it to replace the true system $g(u_k)$. This thereby removes the requirement to perform any identification tests on trial k. Theorem 2 means that Algorithm 1 can be replaced by Algorithm 2 which includes a test to establish whether condition (21) holds. This minimises the number of identification tests, and therefore the overall time taken to track all reference trajectories.

Although (18) stipulates a condition on ILC gain γ which depends on knowledge of the true system, a sufficiently small fixed γ can always be chosen to satisfy (18) without requiring system knowledge. However, since the overall aim is to maximise convergence speed, a larger γ can be chosen and reduced if the sequence of inputs starts to diverge. Also note that a low value of γ is not overly detrimental as it will satisfy the passivity condition in Algorithm 2 more often and therefore avoid frequent experimental identification tests.

It should also be noted that the term $g'(u)^{\top}\bar{g}'(u,\theta) > 0$ is only required to hold for a convex set containing u_k and u_{k+1} . Although g(u) is not known, the condition has practical use since it instructs the designer to add more granularity to the ANN mapping in locations where its gradient may deviate from the true system. The next results illustrate this, and also show advantages in using a simple ANN form for the model $\bar{g}(u,\theta)$.

Theorem 3. Let the system dynamics y = g(u) comprise a monotonic function of each variable, i.e.

$$\forall x, y \in dom(g), \quad \langle (g(x) - g(y)), (x - y) \rangle > 0 \tag{27}$$

in the case that it is increasing, or

$$\forall x, y \in dom(g), \quad \langle (g(x) - g(y)), (x - y) \rangle < 0 \tag{28}$$

in the case it is decreasing. Then a feed-forward neural network $\hat{y} = \bar{g}(u,\theta)$ trained to minimise (26) on a set of Q > m previous plant signals $\{u_i,y_i\}_{i=1,\dots,Q}$, satisfies

$$\mathbf{g}'(\mathbf{u})^{\mathsf{T}}\bar{\mathbf{g}}'(\mathbf{u},\boldsymbol{\theta}) > 0. \tag{29}$$

Algorithm 2 ANN based ILC

Require: Reference set \mathcal{R} , accuracy margin δ , ANN structure $\bar{g}(u, \theta)$ for i = 1: n do

Set k = 0. Select an optimal starting input, u_0 , for reference r_i as

$$\mathbf{u}_0 := \min_{\mathbf{u}} \|\mathbf{r}_i - \bar{\mathbf{g}}(\mathbf{u}, \hat{\boldsymbol{\theta}})\|^2$$
 (25)

while $|J_i(u_k) - J_i(u^*)| < \delta$ do

Apply u_k experimentally, record $y_k = g(u_k)$.

Fit ANN parameter vector θ to all previous experimental data $\{u_i, y_i\}$ (e.g. generated from applying ILC to previous trials and references) by solving

$$\hat{\theta} := \min_{\theta} \sum_{i} \|\mathbf{y}_{i} - \bar{\mathbf{g}}(\mathbf{u}_{i}, \theta)\|^{2}. \tag{26}$$

via back propagation. This can be done recursively by retraining the model on only the new data.

if $\mathbf{g}'(\mathbf{u}_k)^{\top} \bar{\mathbf{g}}'(\mathbf{u}_k, \hat{\boldsymbol{\theta}}) > 0$ holds then

Use the ANN to compute the ILC update (17)

else

Identify $g'(u_k)$ experimentally by applying sufficiently exciting input u and solving (11).

Compute new ILC update using (8).

end if k = k + 1 end while end for

Proof. Consider a neural network with a single hidden layer, which has the form

$$\hat{\mathbf{y}} = W_2 \sigma(W_1 \mathbf{u} + \mathbf{b}_1) + \mathbf{b}_2 \tag{30}$$

where W_1 , W_2 contain the weights, and b_1 , b_2 are bias terms (Gal, 2016). Assuming a rectified linear form for element-wise nonlinearity $\sigma(\cdot)$, this simplifies to

$$\hat{\mathbf{y}} = W_2 W_1 \mathbf{u} + W_2 \mathbf{b}_1 + \mathbf{b}_2 \tag{31}$$

$$=Wu+c\tag{32}$$

where $u \in \mathbb{R}^{mN \times 1}$, $y \in \mathbb{R}^{pN \times 1}$, $W \in \mathbb{R}^{pN \times mN}$ and $c \in \mathbb{R}^{pN \times 1}$. This is also the resulting form for any number of hidden layers. Assume a Euclidean loss function, which corresponds to

$$J(\theta) := \frac{1}{Q} \sum_{i=1}^{Q} \|\mathbf{y}_i - \hat{\mathbf{y}}_i(\mathbf{u}_i, \theta)\|^2.$$
 (33)

Training the network via back propagation is then equivalent to solving

$$\min_{\theta} J(\theta) = \min_{W,c} \left\| \begin{bmatrix} \mathbf{y}_{1}^{\mathsf{T}} \\ \vdots \\ \mathbf{y}_{Q}^{\mathsf{T}} \end{bmatrix} - \begin{bmatrix} 1 & \mathbf{u}_{1}^{\mathsf{T}} \\ \vdots & \vdots \\ 1 & \mathbf{u}_{Q}^{\mathsf{T}} \end{bmatrix} \underbrace{\begin{bmatrix} c^{\mathsf{T}} \\ W^{\mathsf{T}} \end{bmatrix}}_{\theta} \right\|^{2} \tag{34}$$

with solution $\theta^* = (X^T X)^{-1} X^T Y = X^{\dagger} Y$. This can be equivalently expressed using the block matrix pseudoinverse

$$\begin{bmatrix} (P_B^{\perp}A)^{\dagger} \\ (P_A^{\perp}B)^{\dagger} \end{bmatrix} Y \tag{35}$$

with
$$A = \begin{bmatrix} 1 \\ \vdots \\ 1 \end{bmatrix} \in \mathbb{R}^{Q \times 1}$$
, $B = \begin{bmatrix} u_1^\top \\ \vdots \\ u_Q^\top \end{bmatrix} \in \mathbb{R}^{Q \times mN}$. Here $P_A^{\perp} \in \mathbb{R}^{Q \times Q}$ and $P_B^{\perp} \in \mathbb{R}^{Q \times Q}$ are the orthogonal projection matrices onto A and B

respectively. Hence the optimal W, termed W^* , is

$$\begin{split} W^* &= ((P_A^\perp B)^\dagger Y)^\top \\ &= Y^\top (B^\top (P_A^\perp)^\top)^\dagger \\ &= Y^\top (B^\top P_A^\perp)^\dagger \\ &= \left[\begin{array}{ccc} \mathbf{y}_1 & \cdots & \mathbf{y}_Q \end{array} \right] \left(\left[\begin{array}{ccc} \mathbf{u}_1 & \cdots & \mathbf{u}_Q \end{array} \right] P^\perp \\ & \left[\begin{array}{ccc} 1 \\ \vdots \\ 1 \end{array} \right] \right)^\dagger. \end{split}$$

Here $P_A^{\perp} = I - A(A^{\top}A)^{-1}A^{\top}$ so that

$$P^{\perp} \begin{bmatrix} 1 \\ \vdots \\ 1 \end{bmatrix} = \begin{bmatrix} 1 & \cdots & 0 \\ \vdots & \ddots & \vdots \\ 0 & \cdots & 1 \end{bmatrix} - \begin{bmatrix} 1 \\ \vdots \\ 1 \end{bmatrix} \times \begin{bmatrix} 1 \\ \vdots \\ 1 \end{bmatrix} \times \begin{bmatrix} 1 \\ \vdots \\ 1 \end{bmatrix} \begin{bmatrix} 1$$

It follows that

$$W^{*} = \begin{bmatrix} y_{1} & \cdots & y_{Q} \end{bmatrix} \times \\ \begin{bmatrix} u_{1} & \cdots & u_{Q} \end{bmatrix} \begin{bmatrix} (1 - \frac{1}{Q}) & \cdots & -\frac{1}{Q} \\ \vdots & \ddots & \vdots \\ -\frac{1}{Q} & \cdots & (1 - \frac{1}{Q}) \end{bmatrix}^{\dagger} \\ = \frac{\begin{bmatrix} y_{1} & \cdots & y_{Q} \end{bmatrix}}{N \sum_{j=1}^{Q} \sum_{i=1}^{Q} (u_{j} - u_{i})^{\mathsf{T}} (u_{j} - u_{i})} \\ \begin{bmatrix} \sum_{i=1}^{Q} (u_{1} - u_{i}), & \sum_{i=1}^{Q} (u_{2} - u_{i}), & \cdots & \sum_{i=1}^{Q} (u_{Q} - u_{i}) \end{bmatrix}^{\mathsf{T}} \\ = \frac{\sum_{i=1}^{Q} \sum_{j=1}^{Q} (y_{i} - y_{j}) (u_{i} - u_{j})^{\mathsf{T}}}{Q \sum_{i=1}^{Q} \sum_{j=1}^{Q} (u_{j} - u_{i})^{\mathsf{T}} (u_{j} - u_{i})} \end{bmatrix}^{\mathsf{T}}$$

Since the true plant y = g(u) is a monotonic function of each variable, it follows that

$$\forall x, y \quad \langle (g(x) - g(y)), (x - y) \rangle > 0 \tag{38}$$

in the case that it is increasing, or

$$\forall x, y \quad \langle (g(x) - g(y)), (x - y) \rangle < 0 \tag{39}$$

in the case it is decreasing. These correspond to

$$\forall u_i, u_j \quad (g(u_i) - g(u_j))(u_i - u_j)^\top > 0$$

$$\Leftrightarrow (y_i - y_i)(u_i - u_j)^\top > 0$$

$$\tag{40}$$

or

$$\forall \mathbf{u}_i, \mathbf{u}_j \quad (\mathbf{g}(\mathbf{u}_i) - \mathbf{g}(\mathbf{u}_j))(\mathbf{u}_i - \mathbf{u}_j)^\top < 0$$

$$\Leftrightarrow (\mathbf{y}_i - \mathbf{y}_i)(\mathbf{u}_i - \mathbf{u}_j)^\top < 0$$
 (41)

respectively. From (37) it follows directly that

$$(\bar{\mathbf{g}}'(\mathbf{u},\theta))_{i,j} = (W^*)_{i,j} > 0 \tag{42}$$

and

$$(\bar{\mathbf{g}}'(\mathbf{u},\theta))_{i,i} = (W^*)_{i,i} < 0 \tag{43}$$

hold respectively for every pair $\{i, j\}$. The property that y = g(u) is a monotonic, (27) or (28), also means that

$$\left(\frac{\partial g_i(u)}{\partial u_i}\right)_{i,i} > 0 \tag{44}$$

in the case that it is increasing, or

$$\left(\frac{\partial g_i(u)}{\partial u_j}\right)_{i,j} < 0 \tag{45}$$

in the case it is decreasing. Therefore the gradient matrix

$$(\mathbf{g}'(\mathbf{u})^{\mathsf{T}})_{i,j} = \begin{pmatrix} \frac{\partial \mathbf{g}_{1}(\mathbf{u})}{\partial u_{1}} & \dots & \frac{\partial \mathbf{g}_{p}(\mathbf{u})}{\partial u_{1}} \\ \vdots & \ddots & \vdots \\ \frac{\partial \mathbf{g}_{1}(\mathbf{u})}{\partial u_{m}} & \dots & \frac{\partial \mathbf{g}_{p}(\mathbf{u})}{\partial u_{m}} \end{pmatrix}^{\mathsf{T}} > 0$$
 (46)

or

$$(\mathbf{g}'(\mathbf{u})^{\mathsf{T}})_{i,j} = \begin{pmatrix} \frac{\partial g_1(\mathbf{u})}{\partial u_1} & \dots & \frac{\partial g_p(\mathbf{u})}{\partial u_1} \\ \vdots & \ddots & \vdots \\ \frac{\partial g_1(\mathbf{u})}{\partial u_m} & \dots & \frac{\partial g_p(\mathbf{u})}{\partial u_m} \end{pmatrix}^{\mathsf{T}} \right\}_{i,j} < 0$$
 (47)

respectively. In both cases it then follows that (29) holds since the product of two commuting positive (or negative) operators is a positive operator, i.e.

$$\begin{bmatrix} \frac{\partial g_1(u)}{\partial u_1} & \dots & \frac{\partial g_p(u)}{\partial u_1} \\ \vdots & \ddots & \vdots \\ \frac{\partial g_1(u)}{\partial u_m} & \dots & \frac{\partial g_p(u)}{\partial u_m} \end{bmatrix}^{\mathsf{T}} W^* > 0. \quad \Box$$
(48)

Theorem 4. Suppose ANN based ILC is applied to track all references in the set R under the conditions of Theorem 2. Then an upper bound on the total number of trials required to meet the accuracy metrics (k_{δ}, δ) in (6), (7) is

$$k_{\delta} \leq \frac{1}{\delta} \sum_{i=1}^{n} \left\{ \frac{\|\mathbf{u}_{0} - \mathbf{u}_{i}^{*}\|^{2}}{2\gamma} + \frac{\gamma}{2} \sum_{j=0}^{\infty} (\bar{J}_{i}'(\mathbf{u}_{j}, \boldsymbol{\theta}) - J_{i}'(\mathbf{u}_{j}))^{\mathsf{T}} \bar{J}_{i}'(\mathbf{u}_{j}, \boldsymbol{\theta}) \right\}$$
(49)

Proof. Since J_i is convex, it is possible to write

$$J_i(u^*) \ge J_i(u) + J_i'(u)^{\top}(u^* - u) \tag{50}$$

$$J_{i}(u) \le J_{i}(u^{*}) + J_{i}'(u)^{\top}(u - u^{*}). \tag{51}$$

Substituting this into (24) yields

$$J_{i}(\boldsymbol{u}_{k+1}) - J_{i}(\boldsymbol{u}^{*}) \leq \frac{1}{2\gamma} \left(2\gamma J_{i}'(\boldsymbol{u}_{k})^{\top} (\boldsymbol{u}_{k} - \boldsymbol{u}^{*}) - \gamma^{2} a_{k} - \|\boldsymbol{u}_{k} - \boldsymbol{u}^{*}\|^{2} + \|\boldsymbol{u}_{k} - \boldsymbol{u}^{*}\|^{2} \right).$$

Now note that

$$\begin{split} &(\boldsymbol{u}_k - \boldsymbol{u}^* - \gamma \bar{J}_i'(\boldsymbol{u}_k, \boldsymbol{\theta}))^\top (\boldsymbol{u}_k - \boldsymbol{u}^* - \gamma \bar{J}_i'(\boldsymbol{u}_k, \boldsymbol{\theta})) \\ &= \|\boldsymbol{u}_k - \boldsymbol{u}^*\|^2 - 2\gamma \bar{J}_i'(\boldsymbol{u}_k, \boldsymbol{\theta})^\top (\boldsymbol{u}_k - \boldsymbol{u}^*) \\ &\quad + \gamma^2 \bar{J}_i'(\boldsymbol{u}_k, \boldsymbol{\theta})^\top \bar{J}_i'(\boldsymbol{u}_k, \boldsymbol{\theta}) \end{split}$$

so that

$$J_{i}(\mathbf{u}_{k+1}) - J_{i}(\mathbf{u}^{*}) \leq \frac{1}{2\gamma} \Big(\|\mathbf{u}_{k} - \mathbf{u}^{*}\|^{2} - \|\mathbf{u}_{k+1} - \mathbf{u}^{*}\|^{2} - \gamma^{2} \Big(J'_{i}(\mathbf{u}_{k}) - \bar{J}'_{i}(\mathbf{u}_{k}, \theta) \Big)^{\mathsf{T}} \bar{J}'_{i}(\mathbf{u}_{k}, \theta) \Big).$$
(52)

Summing over iterations produces

$$\sum_{j=0}^{\infty} \left(J_i(u_{j+1}) - J_i(u^*) \right)$$

$$\leq \sum_{i=0}^{k} \frac{1}{2\gamma} \left(\|u_j - u^*\|^2 - \|u_{j+1} - u^*\|^2 - \gamma^2 \left(J_i'(u_j) \right) \right)$$

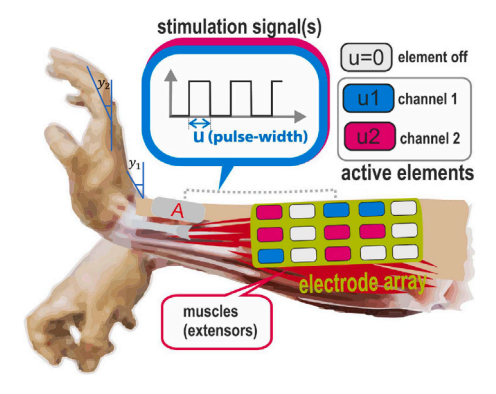


Fig. 2. FES array stimulation of wrist extensors using 2 FES input channels.

$$\begin{split} & - \bar{J}_i'(u_j,\theta) \big)^\top \bar{J}_i'(u_j,\theta) \Big) \\ \leq \frac{\gamma}{2} \sum_{j=0}^k \big(\bar{J}_i'(u_j,\theta) - J_i'(u_j) \big)^\top \bar{J}_i'(u_j,\theta) \\ & + \frac{1}{2\gamma} \|u_0 - u^*\|^2 \end{split}$$

since J_i decreases on every iteration, it can be concluded

$$J_{i}(\mathbf{u}_{k+1}) - J_{i}(\mathbf{u}^{*}) \leq \frac{1}{k} \sum_{j=0}^{k} \left(J_{i}(\mathbf{u}_{j+1}) - J_{i}(\mathbf{u}^{*}) \right)$$

$$\leq \frac{\gamma}{2k} \sum_{j=0}^{k} \left(\bar{J}'_{i}(\mathbf{u}_{j}, \theta) - J'_{i}(\mathbf{u}_{j}) \right)^{\mathsf{T}} \bar{J}'_{i}(\mathbf{u}_{j}, \theta)$$

$$+ \frac{\|\mathbf{u}_{0} - \mathbf{u}^{*}\|^{2}}{2\gamma k}$$
(53)

The summation term in (53) reduces as $\bar{g}(u, \theta)$ more closely approximates the true system g(u), and attains a finite value when $k \to \infty$. Hence taking the limit and rearranging gives the bound (49). \square

Theorem 4 therefore quantifies how the number of trials required for convergence depends on the accuracy of the model. Since model fitting improves as more experimental data are generated, it follows that new references are tracked progressively faster.

5. Numerical results

The ANN based ILC approach is now evaluated on a rehabilitation problem, in which FES is applied to an electrode array in order to produce a set of four hand gestures. The model is based on Theodorou, Todorov, and Valero-Cuevas (2011) and comprises a 3link wrist and hand representation, including radius, metacarpal and phalangeal bones. The FES array elements are chosen to stimulate Flexor Digitorum Profundus and Extensor Communis muscles (u_1 , u_2 respectively). The resultant force is transmitted via a longitudinally symmetric tendon rhombus network (with 5 active and 3 passive tendons) which actuates the wrist and metacarpal-phalangeal joints $(y_1, y_2 \text{ respectively, in degrees})$. This m = 2, p = 2 system accurately models the response to FES, and the clinical aim is to achieve functional gestures such as 'open hand', 'pointing' or 'pinching'. This matches the set-up used with patients in previous studies (Freeman, 2014, 2016; Ward et al., 2020). As in these studies, N = 1 is chosen together with a large sample time, since the purpose is to track the final gesture position. A set of n = 4 references is chosen to provide varied training, given by $\mathbf{r}_1 = [10, 50]^{\mathsf{T}}$, $\mathbf{r}_4 = [70, 70]^{\mathsf{T}}$, $\mathbf{r}_3 = [20, 10]^{\mathsf{T}}$ and $\mathbf{r}_4 = [30, 50]^{\mathsf{T}}$ (see Fig. 2).

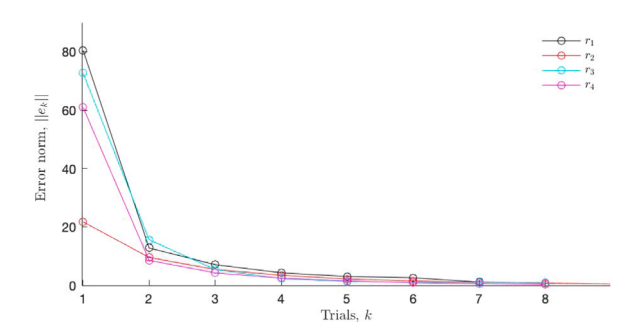


Fig. 3. Convergence of tracking error norm using standard ILC.

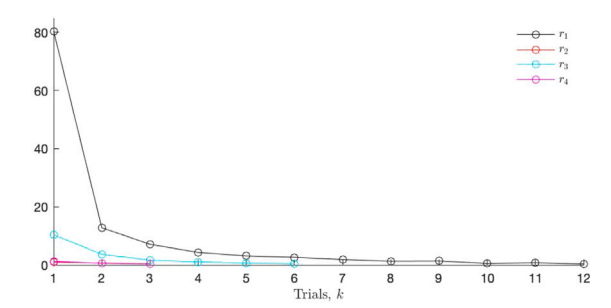


Fig. 4. Convergence of tracking error norm using ANN based ILC.

5.1. Standard gradient ILC

First standard gradient ILC is applied using Algorithm 1 and a stopping criterion of $\delta=0.25$ and initial input $u_0=[0,0]^{\mathsf{T}}$. The error norm results are shown in Fig. 3. In total 34 ILC trials are required, each requiring 3 separate tests to perform. If applied experimentally, this equates to 102 tests in total. This is clearly too many for a typical therapy session.

5.2. Artificial neural network based ILC

ANN based ILC is next applied using Algorithm 2 and the same stopping criterion. Here $\bar{\mathbf{g}}(u,\theta)$ is chosen as an M=1 layer, M_1 neuron ANN with a back-propagation training function that minimises the MSE. Different M_1 values are used in order to compare their ability to fit the known data points and also extrapolate to predict unknown data points. The simulations were performed using the 'feedforwardnet' feedforward neural network structure from the Matlab Deep Learning Toolbox (Matlab R2024a).

Fig. 4 shows the error norm results with M=1 hidden layers and $M_1=4$ neurons. Here a total of 24 ILC trials are required, however, only 9 of these required identification of a new model, with the remainder using ANN model update (17) to generate the next update step. This means only 42 experimental inputs would be needed in practice to track all references. Compared with standard ILC's 102 overall inputs, the improvement is 59%.

Table 1 shows the accuracy using different numbers of neurons and it is clear that only four are sufficient to fit the data in this application. More than ten neurons overfits the data. To illustrate how this is achieved, $\bar{g}(u,\hat{\theta})$ is shown in Fig. 5 immediately after completing r_1 tracking.

6. Experimental results

The hardware used consists of a tracking sensor, user interface software running on a laptop, a control unit, a 24 channel FES electrode array sleeve and FES electronics. The components are shown in Fig.

Table 1 The accuracy of ANN with different number of neurons M_1 .

Neurons, M_1	r_1	r_2	<i>r</i> ₃	r_4	Ident'n trials	Overall inputs	Improvement Percentage
1	9	9	3	2	13	49	52%
2	13	10	3	2	12	52	49%
4	12	3	6	3	9	42	59%
6	12	11	2	4	12	53	48%
10	16	14	2	4	10	56	45%
20	20	17	9	7	15	83	19%
100	20	20	20	5	21	107	-5%

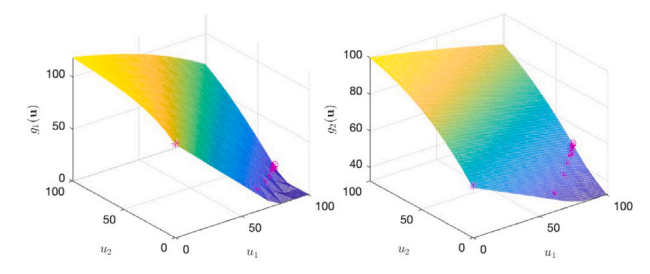


Fig. 5. Plots of $y_1 = \bar{g}_1(u, \hat{\theta})$ and $y_2 = \bar{g}_2(u, \hat{\theta})$ with all points $\{u_k, y_k\}$ after completing r_1 .

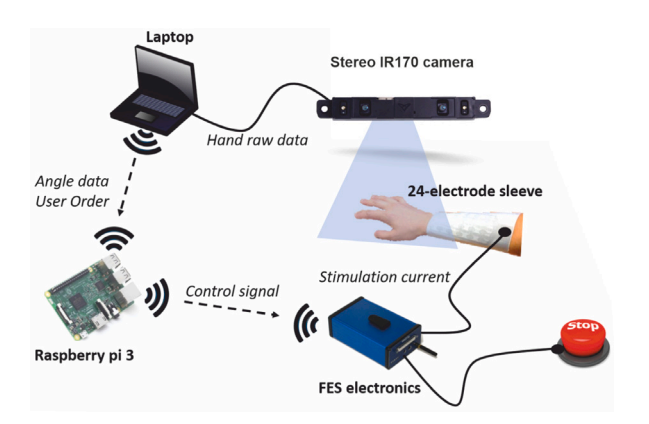


Fig. 6. Upper limb stroke rehabilitation hardware.

6. The sensor (Stereo IR 170 camera, UltraLeap) is a next-generation optical hand tracking module with a $170 \times 170^\circ$ field of view, which collects the positional data of the hand and wrist, and is then processed by the user interface to generate angle data. This is sent to the control unit (Raspberry Pi 4) via wireless transmission, which runs the real-time controller (at 40 Hz). The controller computes the voltage pulse train applied to each element of the 24 channel electrode array. Here, the frequency and amplitude of each pulse train are fixed, and the pulse width of each pulse train is the controlled variable (0–100 μ s). The sensor provides 12 joint angles, however only those corresponding to wrist flexion/extension and the index finger metacarpal-phalangeal joint flexion/extension are used. This matches the set-up of Section 5.

Since the Deep Learning Toolbox is not supported by the Raspberry Pi Simulink toolbox in Matlab R2024a, the ANN was re-implemented using basic functions as a back propagation neural network. A sigmoid was selected as the activation function of the hidden layer, and a linear function as the activation function of the output layer. The learning rate was 0.1 and 1000 training episodes were used.

The simulation tests are now repeated experimentally in a study with eight unimpaired participants (University of Southampton Ethics No. 72855). These participants will be denoted P1, P2, ..., P8 and their details are shown in Table 2.

The experimental setup is shown in Fig. 7. The electrode array was first positioned on the forearm of the participant's dominant arm.

Table 2 Participant demographic information.

No.	Age	Gender	Test arm
P1	36	M	right
P2	21	F	right
P3	46	F	right
P4	45	M	left
P5	31	M	right
P6	55	F	right
P7	36	M	right
P8	37	F	right





Fig. 7. Electrode array, stimulator and Stereo IR 170 camera.

Two stimulation sites were selected from the array, to correspond with activating the Flexor Digitorum Profundus and Extensor Communis muscles. Then a 100 μs FES signal was applied to each of the two channels in turn. While stimulated, the voltage amplitude was slowly increased until a comfortable limit was reached. The pulsewidth was then reset to 0 μs and the amplitude was then fixed for each channel in all remaining tests.

Three reference gestures which include open hand, pointing, and pitch gestures, were used: open hand (with wrist and index finger extended), pinch (with wrist extended and index finger flexed), and horizontal pointing (with wrist partially extended and index finger fully extended). These are denoted \mathbf{r}_1 , \mathbf{r}_2 and \mathbf{r}_3 respectively. The values for participant P1 are $\mathbf{r}_1 = [-33.5, 22.2]^{\mathsf{T}}$, $\mathbf{r}_2 = [33.6, -2.5]^{\mathsf{T}}$ and $\mathbf{r}_3 = [-40.4, 22.6]^{\mathsf{T}}$ with unit in degrees, and a positive value corresponding to flexion for each angle.

Following this, the standard ILC and ANN based ILC algorithms introduced in Sections 3 and 4 were applied. During each test, the participant was instructed to apply no voluntary effort, and they were not shown the reference movement. Note that omitting voluntary effort in the controller design has been assumed in all clinical trials using ILC (Freeman, Exell, Meadmore, Hallewell, & Hughes, 2015). This is because patients are typically highly impaired with significant weakness and so their voluntary input is minimal starting rehabilitation. Instead, their voluntary effort is treated as an external disturbance. A time of ten seconds was added between trials so that the participant's hand naturally returned to the same starting condition under the effect of gravity and zero applied stimulation.

As in the previous ILC applications of Freeman (2014) and Yang et al. (2018), N=1 was selected and the stimulation inputs were smoothly applied to each array element using a ramp signal of three seconds duration. The resulting hand gesture was measured.

In the previous section, the stopping criteria $|J_i(u_k)-J_i(u^*)|<\delta$ was used. During experiments, the value $J_i(u^*)$ is not known, and so it is assumed that perfect tracking is possible, $J_i(u^*)=0$. This corresponds to the stopping criteria $|J_i(u_k)-J_i(u^*)|=\|e_k\|^2<\delta$. A value of $\delta=5$ was selected as it corresponds to accurate tracking (i.e. joint angle error norm less than $\sqrt{5}$ degrees) that is considered practically achievable.

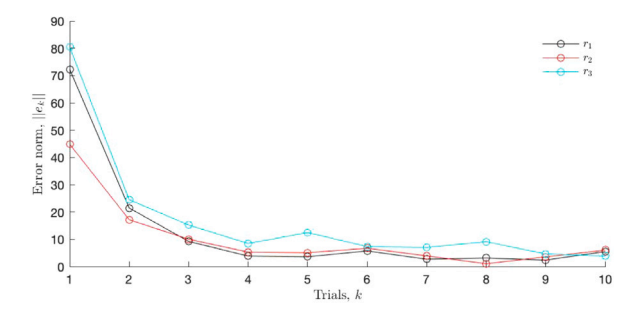


Fig. 8. Convergence of tracking error norm using standard ILC with $\gamma = 2$ for P1, (experimental results).

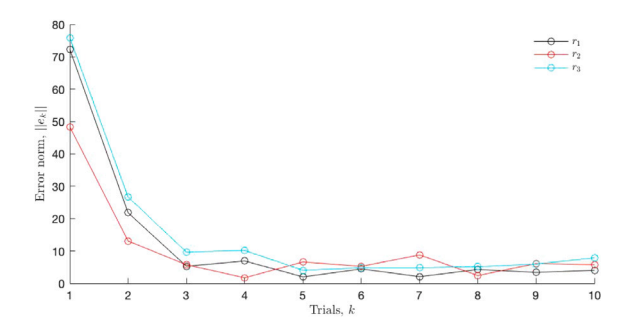


Fig. 9. Convergence of tracking error norm using standard ILC with $\gamma=10$ for P1, (experimental results).

The minimum number of trials to achieve this criteria will be termed the 'total trials', however the experiments will still be continued for ten trials in order to determine whether the level of error is maintained.

6.1. Standard ILC

First, standard ILC was applied as described in Algorithm 1 of Section 3. Two system gains were used for all participants: $\gamma=10$ and $\gamma=2$. Results for participant P1 are shown in Fig. 8 for $\gamma=2$. These confirm convergence to a low level of error for all three references.

Further convergence results for participant P1 are shown in Fig. 9 using $\gamma = 10$. These demonstrate slightly faster convergence with high accuracy maintained over the ten trials.

For each reference, the number of trials required to meet the stopping criteria is listed in Table 3 for all participants. The total number of trials requiring identification, termed 'identification trials', is also shown, together with the total number of inputs (i.e. 3 inputs for each identification trial and 1 input for each of the remaining trials). Since this is standard ILC, all trials require identification. In almost all cases the increased ILC gain increases the convergence speed, however a large number of experiments is always required.

6.2. Artificial neural network based ILC

As in Section 5.2, Algorithm 2 was next applied with the same parameters as the standard ILC method. ANN parameter choices $M=1, M_1=1$ and $M=1, M_1=4$ were tested for all participants.

The error norm results for participant P1 using ANN based ILC with $\gamma=2$ and $M_1=1$ are shown in Fig. 10. The convergence speed of ANN based ILC is faster than standard ILC, since the later references start from a smaller initial error norm due to the use of the fitted model $\bar{g}(u,\hat{\theta})$. A total of 13 ILC trials are required, however, only 10 of these require the identification of a new model, with the remainder using parameterised model update (17) to generate the next update step. This led to only 33 experimental inputs being needed to track all

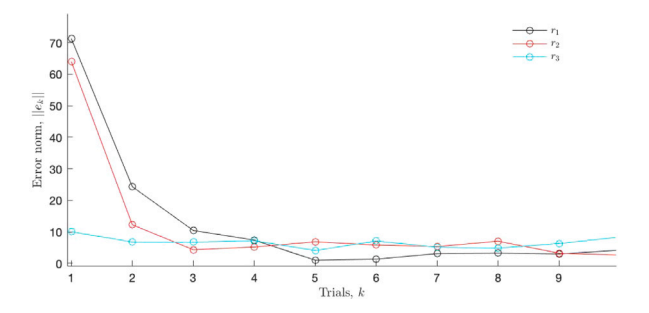


Fig. 10. Convergence of tracking error norm using ANN based ILC with $\gamma = 2$ and $M_1 = 1$ for P1, (experimental results).

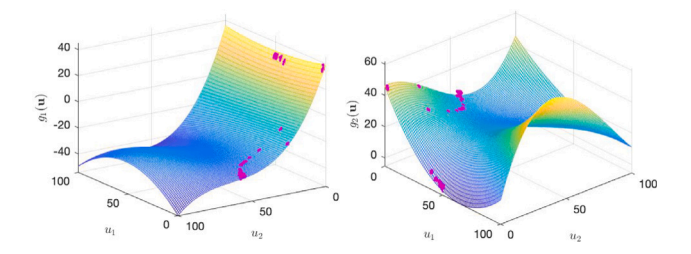


Fig. 11. Participant P1 results with $\gamma = 2$. Plots of $y_1 = \bar{g}_1(u, \hat{\theta})$ and $y_2 = \bar{g}_2(u, \hat{\theta})$ with all ILC points $\{u_k, y_k\}$ after completing r_1 , (experimental results).

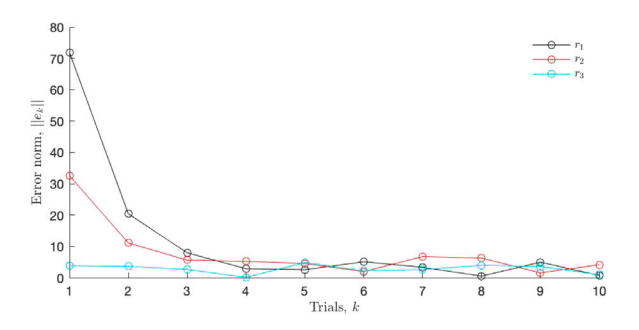


Fig. 12. Convergence of tracking error norm using ANN based ILC with $\gamma = 10$, $M_1 = 1$ for P1, (experimental results).

three references. This equates to (60-33)/60=45% fewer experiments compared to Standard ILC. To show how this was achieved, the fitted model $\bar{\mathbf{g}}(u,\hat{\boldsymbol{\theta}})$ is shown in Fig. 11 immediately after completing tracking of r_1 .

Results using $\gamma=10$, $M_1=1$ are shown in Fig. 12 for participant P1. These show even faster convergence with only 20 experimental inputs.

The sequence of FES inputs applied is shown in Fig. 13 for $\gamma=2$, and Fig. 14 for $\gamma=10$.

For each reference, the overall total number of experimental inputs is listed in Table 4 for all participants. In all cases there is significant improvement in terms of a reduced number of experiments required to achieve the three gestures.

The average improvement over all participants is (55.5 - 24.6)/55.5 = 56%, meaning that the total test time is less than half.

7. Conclusions

An ANN based ILC approach has been developed to reduce the experimental overhead required by existing model-free/data-driven ILC approaches. This uses all prior data to fit an ANN model which is used to construct the next ILC update. Conditions for convergence to minimal error are derived which inform model design, minimising the

Table 3 Total trials required by Standard ILC for all participants. Average number of inputs: 68.2 for $\gamma = 2$, 55.5 for $\gamma = 10$.

Trials Test						
Participant	γ	r_1	r_2	<i>r</i> ₃	Ident'n trials	Overall inputs
P1	2	4	7	9	20	60
	10	5	4	5	14	42
P2	2	7	7	10	24	72
	10	6	4	7	17	51
P3	2	8	5	10	23	69
	10	7	3	10	20	60
P4	2	5	6	10	21	63
	10	10	4	10	24	72
P5	2	10	9	10	29	87
	10	5	10	10	25	75
P6	2	10	6	10	26	78
	10	4	3	8	15	45
P7	2	6	5	9	20	60
	10	4	4	8	16	48
P8	2	5	5	9	19	57
	10	4	5	8	17	51

Table 4 Total trials required by ANN based function ILC for all participants. Improvement denotes the fraction of required inputs compared with standard ILC. Average number of inputs: 26.7 for $M_1 = 1$, $\gamma = 2$, 24.6 for $M_1 = 1$, $\gamma = 10$, 35.6 for $M_1 = 4$, $\gamma = 2$, 25.6 for $M_1 = 4$, $\gamma = 10$.

Trials Test	M_1		_	_	_	Ident'n trials	Overall inputs	Improvement
Participant	<i>M</i> ₁	γ	r_1	r_2	<i>r</i> ₃	ident ii tiiais	Overall inputs	miprovemen
P1	1	2	5	3	5	10	33	45%
	1	10	4	5	1	5	20	52%
	4	2	5	5	10	16	52	13%
	4	10	4	3	2	5	19	55%
P2	1	2	4	4	3	4	19	74%
	1	10	6	3	1	7	24	53%
	4	2	5	8	3	13	42	42%
	4	10	4	4	3	4	19	63%
Р3	1	2	4	3	3	9	28	59%
	1	10	3	2	3	5	18	70%
	4	2	4	6	4	11	36	48%
	4	10	5	8	1	5	24	60%
P4	1	2	4	8	7	4	27	57%
	1	10	4	2	1	4	15	79%
	4	2	8	3	6	8	33	48%
	4	10	5	5	1	5	21	71%
P5	1	2	5	5	1	7	25	71%
	1	10	6	3	10	16	51	32%
	4	2	10	5	10	10	45	48%
	4	10	10	3	4	10	37	51%
P6	1	2	6	10	1	12	41	47%
	1	10	5	4	8	5	27	40%
	4	2	7	6	1	7	28	64%
	4	10	6	3	8	9	35	22%
P7	1	2	4	4	2	4	18	70%
	1	10	5	2	6	5	23	52%
	4	2	4	4	6	6	24	60%
	4	10	6	3	3	6	24	50%
P8	1	2	5	3	4	6	23	59%
	1	10	4	4	2	5	19	63%
	4	2	5	4	5	6	25	56%
	4	10	5	2	6	8	26	49%

number of identification tests while preserving convergence. The framework is demonstrated on a key biomedical control problem, where it is shown that it reduces the experiments required to a number that is clinically feasible (from 55.5 to 24.6 on average). This opens up the possibility of translating effective FES based therapy to clinics and

patients' own homes. Future work will evaluate the approach with stroke participants.

It has been assumed that the ANN used to fit the measured data is of a generic form that does not embed any knowledge of the underlying

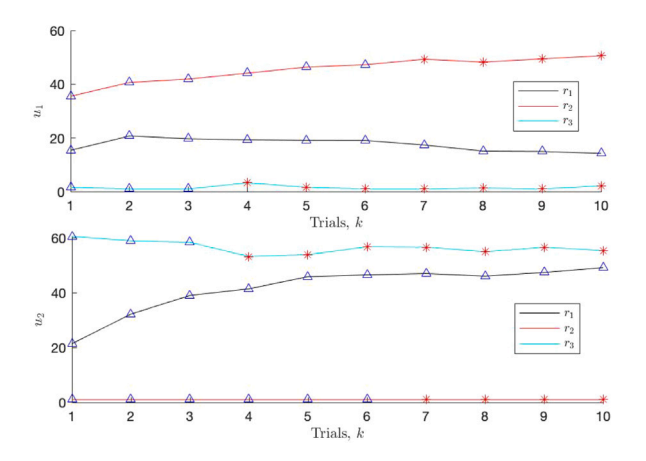


Fig. 13. Participant P1 results with $\gamma = 2$, showing stimulation input signals, where \triangle denotes ILC updates requiring experimental identification step, (experimental results).

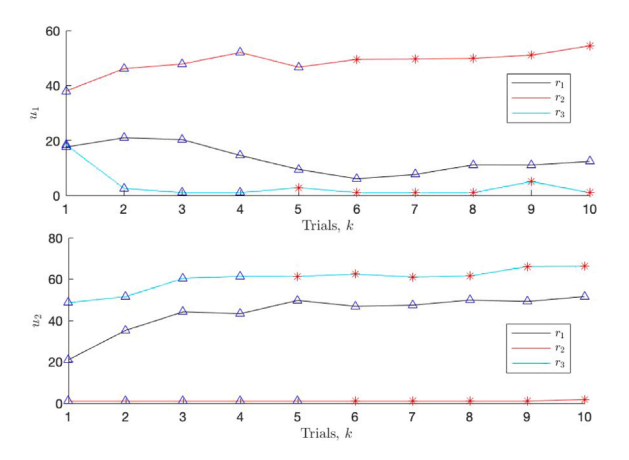


Fig. 14. Participant P1 results with $\gamma=10$ showing stimulation input signals, where \triangle denotes ILC updates requiring experimental identification step, (experimental results).

system. While this is convenient for most applications, it is also possible to use the same model $\bar{\mathbf{g}}(u,\theta)$ to capture a parameterised model, for example musculoskeletal dynamics capturing stimulated hand and wrist dynamics (Soska, 2014). In this case θ contains the unknown parameters, and its small dimension may lead to faster convergence. The possible benefits of this approach will be evaluated in the future study with stroke participants.

Technical development will also focus on incorporating automatic step size adaptation schemes to further optimise the trade-off between convergence speed and robustness.

CRediT authorship contribution statement

Xiaoru Sun: Writing – original draft, Software, Methodology, Conceptualization. **Chris T. Freeman:** Writing – review & editing, Supervision, Methodology.

Declaration of competing interest

The authors declare that they have no known competing financial interests or personal relationships that could have appeared to influence the work reported in this paper.

References

- Ballester, B. R., Ward, N. S., Brander, F., Maier, M., Kelly, K., & Verschure, P. F. M. J. (2022). Journal of neurology, neurosurgery, and psychiatry. Relationship Between Intensity and Recovery in Post-Stroke Rehabilitation: A Retrospective Analysis, 93, 226–228.
- Bijelić, G., Popović-Bijelić, A., Jorgovanović, N., Bojanić, D., & Popović, D. B. (2004).
 E actitrode: The new selective stimulation interface for functional movements in hemiplegics patients. Serbian Journal of Electrical Engineering, 1, 21–28.
- Chen, F., & Wen, C. (2020). Neural-network-based robust iterative learning control for nonlinear systems with randomly varying trial lengths. *IEEE Transactions on Neural Networks and Learning Systems*, 31, 1884–1896. http://dx.doi.org/10.1109/TNNLS. 2019.2911095
- Chi, R. H., Hou, Z. S., Huang, B., & Jin, S. T. (2015). A unified data-driven design framework of optimality-based generalized iterative learning control. *Computers & Chemical Engineering*, 77, 10–23.
- Chi, R. H., Hou, Z. S., Jin, S. T., & Huang, B. (2018). Computationally efficient datadriven higher order optimal iterative learning control. *IEEE Transactions on Neural Networks and Learning Systems*, 29, 5971–5980.
- Chi, R., Li, H., Lin, N., & Huang, B. (2024). Data-driven indirect iterative learning control. IEEE Transactions on Cybernetics, 53, 1650–1660.
- Crow, J., & Smith, A. (2023). National clinical guideline for stroke for the United Kingdom and Ireland: Part I-an overview of the updated recommendations. British Journal of Occupational Therapy, Article 03080226231188020.
- De Marchis, C., Santos Monteiro, T., Simon-Martinez, C., Conforto, S., & Gharabaghi, A. (2016). Multi-contact functional electrical stimulation for hand opening: Electrophysiologically driven identification of the optimal stimulation site. *Journal of Neuroengineering and Rehabilitation*, 13, 1–9.
- Eraifej, J., Clark, W., France, B., Desando, S., & Moore, D. (2017). Effectiveness of upper limb functional electrical stimulation after stroke for the improvement of activities of daily living and motor function: A systematic review and meta-analysis. Systematic Reviews, 6, 1–21.
- Feigin, V. L., Brainin, M., Norrving, B., Martins, S., Sacco, R. L., Hacke, W., et al. (2022). World stroke organization (WSO): Global stroke fact sheet 2022. *International Journal of Stroke*, 17, 18–29.
- Freeman, C. T. (2014). Electrode array-based electrical stimulation using ILC with restricted input subspace. *Control Engineering Practice*, 23, 32–43.
- Freeman, C. T. (2016). Control system design for electrical stimulation in upper limb rehabilitation. (pp. 1–189). Springer international publishing, http://dx.doi.org/10. 1007/978-3-319-25706-8.
- Freeman, C. T., Exell, T., Meadmore, K., Hallewell, E., & Hughes, A.-M. (2015). Computational models of upper-limb motion during functional reaching tasks for application in FES-based stroke rehabilitation. *Biomedical Engineering*, 60, 179–191.
- Freeman, C. T., Hughes, A.-M., Burridge, J. H., Chappell, P. H., Lewin, P. L., & Rogers, E. (2009). A model of the upper extremity using FES for stroke rehabilitation. *Journal of Biomechanical Engineering*, 131, Article 031011.
- Gal, Y. (2016). Uncertainty in deep learning (Ph.D. thesis), University of Cambridge.
- He, S., Chen, W., Li, D., Xi, Y., Xu, Y., & Zheng, P. (2022). Iterative learning control with data-driven-based compensation. *IEEE Transactions on Cybernetics*, 52, 7402–7503
- Hoffmann, U., Deinhofer, M., & Keller, T. (2012). Automatic determination of parameters for multipad functional electrical stimulation: Application to hand opening and closing. In 2012 annual international conference of the IEEE engineering in medicine and biology society (pp. 1859–1863). IEEE.
- Hu, Y., Zhang, C., Wang, B., Zhao, J., Gong, X., Gao, J., et al. (2024). Noise-tolerant ZNN-based data-driven iterative learning control for discrete nonaffine nonlinear MIMO repetitive systems. IEEE/CAA Journal of Automatica Sinica, 11, 344–361.
- Huang, L., & Huang, H. (2024). Improved data-driven high-order model-free adaptive iterative learning control with fast convergence for trajectory tracking systems. *Transactions of the Institute of Measurement and Control*, 46, 2884–2896.
- Hughes, A.-M., Burridge, J. H., Demain, S. H., Ellis-Hill, C., Meagher, C., Tedesco-Triccas, L., et al. (2014). Translation of evidence-based assistive technologies into stroke rehabilitation: Users' perceptions of the barriers and opportunities. BMC Health Services Research, 14, 1–12.
- Huo, B., Freeman, C. T., & Liu, Y. (2020). Data-driven gradient-based point-to-point iterative learning control for nonlinear systems. *Nonlinear Dynamics*, 102, 269–283.
- Imatz-Ojanguren, E., Irigoyen, E., Valencia-Blanco, D., & Keller, T. (2016). Neurofuzzy models for hand movements induced by functional electrical stimulation in able-bodied and hemiplegic subjects. *Medical Engineering & Physics*, 38, 1214–1222.
- Intercollegiate Stroke Working Party; London (2023). National clinical guideline for stroke for the UK and Ireland. URL: www.strokeguidelines.org.
- Lee, Y.-H., Cheng, Y.-T., Yuan, K.-S., & Tsao, T.-C. (2025). Data-driven iterative learning control for nonlinear multivariate systems using transpose adaptive filtering. *European Journal of Control*, 85, Article 101273.
- Lee, Y.-H., Rai, S., & Tsao, T.-C. (2022). Data-driven iterative learning control of nonlinear systems by adaptive model matching. *IEEE/ASME Transactions on Mechatronics*, 27, 5626–5636.
- Lin, T., Owens, D. H., & Hätönen, J. (2006). Newton method based iterative learning control for discrete non-linear systems. *International Journal of Control*, 79, 1263–1276.

- Liu, T., Wang, D., & Chi, R. (2015). Neural network based terminal iterative learning control for uncertain nonlinear non-affine systems. *International Journal of Adaptive Control and Signal Processing*, 29, 1274–1286.
- Malešević, N. M., Maneski, L. Z. P., Ilić, V., Jorgovanović, N., Bijelić, G., Keller, T., et al. (2012). A multi-pad electrode based functional electrical stimulation system for restoration of grasp. Journal of Neuroengineering and Rehabilitation, 9, 1–12.
- Maneski, L. P., Topalović, I., Jovičić, N., Dedijer, S., Konstantinović, L., & Popović, D. B. (2016). Stimulation map for control of functional grasp based on multi-channel EMG recordings. Medical Engineering & Physics, 38, 1251–1259.
- Marquez-Chin, C., Kapadia-Desai, N., & Kalsi-Ryan, S. (2021). Functional electrical stimulation therapy: A closer look. In Brain-computer interfaces: Neurorehabilitation of voluntary movement after stroke and spinal cord injury (pp. 11–25). Springer.
- O'Dwyer, S. B., O'Keeffe, D. T., Coote, S., & Lyons, G. M. (2006). An electrode configuration technique using an electrode matrix arrangement for FES-based upper arm rehabilitation systems. *Medical Engineering & Physics*, 28, 166–176.
- Owens, D. H., Freeman, C. T., & Chu, B. (2014). An inverse-model approach to multivariable norm optimal iterative learning control with auxiliary optimisation. *International Journal of Control*, 87, 1646–1671. http://dx.doi.org/10.1080/ 00207179.2014.880951.
- Popović, D. B., & Popović, M. B. (2009). Automatic determination of the optimal shape of a surface electrode: Selective stimulation. *Journal of Neuroscience Methods*, 178, 174–181.
- Popović-Maneski, L., Kostić, M., Bijelić, G., Kelle, T., Mitrović, S., Konstantinović, L., et al. (2013). Multi-pad electrode for effective grasping: Design. IEEE Transactions on Neural Systems and Rehabilitation Engineering, 21, 648–654.
- Saposnik, G., Galanos, L. C., Guerrero, R., Casagrande, F., Adhamidhis, E., Gao, M. M. Y., et al. (2022). The world stroke academy: A world stroke organization global pathway to improve knowledge in stroke care. *International Journal of Stroke*, 17, 829–834
- Schill, O., Rupp, R., Pylatiuk, C., Schulz, S., & Reischl, M. (2009). Automatic adaptation of a self-adhesive multi-electrode array for active wrist joint stabilization in tetraplegic SCI individuals. In 2009 IEEE Toronto international conference science and technology for humanity (pp. 708–713). IEEE.

- Soleimani, E., Sedigh, A. K., & Nikoofard, A. (2025). Data-driven reinforcement learning-based forgetting factor iterative learning control. *IEEE Transactions on Automation Science and Engineering*, 22, 12245–12256.
- Soska, A. (2014). Surface electrode array-based electrical stimulation and iterative learning control for hand rehabilitation (Ph.D. thesis), University of Southampton.
- Stockley, R., Peel, R., Jarvis, K., & Connell, L. (2019). Current therapy for the upper limb after stroke: A cross-sectional survey of UK therapists. *British Medical Journal*, 9
- Sun, X., & Freeman, C. T. (2024a). Artificial neural network based ILC with application to stroke rehabilitation. In 2024 American control conference (pp. 4825–4830). IEEE.
- Sun, X., & Freeman, C. T. (2024b). Parameterised function ILC with application to stroke rehabilitation. Control Engineering Practice, 145, Article 105878.
- Theodorou, E., Todorov, E., & Valero-Cuevas, F. J. (2011). Neuromuscular stochastic optimal control of atendon driven index finger model. In American control conference.
- Tian, Z., Yu, S., Chen, Q., Yang, F., Wang, J., Liu, J., et al. (2025). A data-driven feedforward control combining feedforward tuning and cascaded iterative learning control. *Measurement*, 253, Article 117414.
- Wang, Y.-C., & Chien, C.-J. (2012). Repetitive tracking control of nonlinear systems using reinforcement fuzzy-neural adaptive iterative learning controller. Applied Mathematics & Information Sciences, 6, 475–482.
- Ward, T., Grabham, N., Freeman, C., Wei, Y., Hughes, A.-M., Power, C., et al. (2020).
 Multichannel biphasic muscle stimulation system for post stroke rehabilitation.
 Electronics. 9, 1156.
- Xu, K., Meng, B., & Wang, Z. (2024). Generalized regression neural networks-based data-driven iterative learning control for nonlinear non-affine discrete-time systems. *Expert Systems with Applications*, 248, Article 123339.
- Yang, K., Meadmore, K., Freeman, C., Grabham, N., Hughes, A.-M., Wei, Y., et al. (2018). Development of user-friendly wearable electronic textiles for healthcare applications. Sensors, 18, 2410.
- Zhang, Z., & Zou, Q. (2024). Data-driven robust iterative learning control of linear systems. Automatica, 164, Article 111646.
- Zhu, Y., & Hou, Z. (2014). Data-driven MFAC for a class of discrete-time nonlinear systems with RBFNN. IEEE Transactions on Neural Networks and Learning Systems, 25. 5.